The influence of nanostructured features on bacterial adhesion and bone cell functions on severely shot peened 316L stainless steel

Sara Bagherifard [a, b, c, *], Daniel J. Hickey [d], Alba C. de Luca [c], Vera N. Malheiro [c], Athina E. Markaki [c], Mario Guagliano [a], Thomas J. Webster [d, e]

[a] *Department of Mechanical Engineering, Politecnico di Milano, Milan, Italy*
[b] *Harvard-MIT Division of Health Sciences and Technology, Massachusetts Institute of Technology, Cambridge, MA, USA*
[c] *Department of Engineering, University of Cambridge, Cambridge, UK*
[d] *Department of Chemical Engineering, Northeastern University, Boston, MA, USA*
[e] *Center of Excellence for Advanced Materials Research, King Abdulaziz University, Jeddah, Saudi Arabia*

Received 20 May 2015
Received in revised form
7 September 2015
Accepted 10 September 2015
Available online 12 September 2015

1. Introduction

Biophysical signals present in cellular microenvironments are known to significantly affect cellular activities. Surface micro-/nano-scale topography, grain structure, and substrate stiffness have been confirmed to modulate cellular functions at the cell-substrate interface [1–6]. Bacterial adhesion and biofilm formation can also be directly affected by mechanical cues, in some cases even to a greater degree compared to that induced through chemical signals [7,8]. Biofilms are communities of bacteria formed on a surface that can pose persistent pathogenic threats due to their extreme antibiotic resistance and reducing the risk of their formation is of the utmost importance.

Greater appropriate cell activities can be of significant importance to promote bone tissue formation and osseointegration on

* Corresponding author. Department of Mechanical Engineering, Politecnico di Milano, Milan, Italy.
E-mail address: sara.bagherifard@polimi.it (S. Bagherifard).

metallic biomaterial surfaces, whilst decreasing bacteria adhesion to the substrate can reduce the risk of undesirable infection and costly successive complications including revision surgeries. The mechano-selective adhesion of cells and bacteria to substrates and their potential to enhance the success rate of metallic implants have brought growing attention to a wide variety of surface modification approaches. Among the applied techniques, severe plastic deformation (SPD) processes are gaining increasing interest due to their ability to induce advanced mechanical and physical characteristics on the treated material through grain refinement. SPD methods have been described as metal forming processes that result in exceptional grain refinement by imposing high strain rates at relatively low temperatures without considerably altering the overall dimensions of the material [9,10].

Severe shot peening (SSP) can be described as one of the most effective and, at the same time, the least demanding SPD techniques. SSP is based on impacting the material surface with high energy shots as demonstrated in Fig. 1; the shot size and material are chosen based on the application of interest. SSP is derived from conventional air blast shot peening and can be performed using the same apparatus, by applying a particular set of peening parameters to enhance the impact kinetic energy and thereby introduce numerous defects, dislocations and grain boundaries onto the surface layer of a material, subsequently transforming the coarse grained structure into a nanostructured one [11,12]. A significant advantage of SSP in contrast with many other SPD techniques is that SSP does not involve geometrical restrictions for surface nanocrystallization. The characteristics of the affected surface layer in terms of grain size, thickness, surface roughness, and work hardening as well as induced residual stresses can be tailored by the proper choice of peening parameters. Almen intensity (a measure of shot stream kinematic energy during the shot peening process) and surface coverage (the ratio of the area covered by plastic indentation to the whole surface area) are the major peening parameters that insure the repeatability and facilitate the control of process effects. Studies performed on SSP in recent years have indicated its ability to significantly improve the mechanical prop-erties of treated materials in terms of hardness, fatigue strength, corrosion, wear, scratch resistance and so on, contributing to enhanced functionality and service characteristics of the material [13,14].

316L stainless steel (the most widely used stainless steel for orthopedic, cardiovascular and craniofacial applications due to its good corrosion resistance and formability [15]) was therefore used to assess the interaction between the treated surfaces and human osteoblasts (bone forming cells), as well as a range of microorganisms, including the gram-positive strains *Staphylococcus aureus* and *Staphylococcus epidermidis,* and gram negative *Pseudomonas aeruginosa* and ampicillin-resistant *Escherichia coli*. The experiments were directed to evaluate the potential application of SSP treatment to fabricate multifunctional bio-implant materials with enhanced mechanical characteristics and biocompatibility. The growing resistance of bacteria to conventional antibiotics, the need for developing advanced orthopedic implants with improved biocompatibility, along with the necessity of using a mechanically strong material to withstand physiological strains and stresses, gave the initial impetus for the development of advanced multifunctional materials for bone implants.

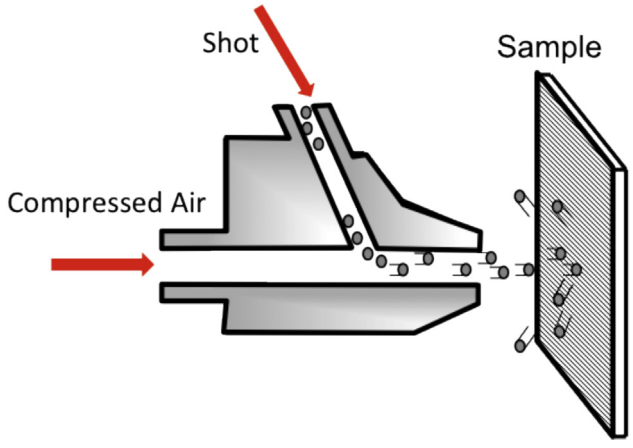

Fig. 1. Schematic of the shot peening apparatus.

To examine the effects of grain size refinement alone (without the confounding changes in roughness), a group of samples were surface-ground after the SSP treatments to remove differences in surface roughness between sample groups. The mechanical and physical properties of the substrates were characterized by microstructural observation, microhardness measurements, X-ray diffraction (XRD) grain size and residual stress measurements, as well as atomic force microscopy (AFM), interferometric profilometry, and water contact angle measurements. The short term response of human osteoblasts seeded onto different sample groups was assessed in terms of adhesion, proliferation, morphology and spreading. The early adhesion and growth of *S. aureus*, *Pseudomonas aeruginosa*, *S. epidermidis* and ampicillin-resistant *E. coli* was also measured by colony count assays. Results showed, for the first time, significant promise to enhance the mechanical and cytocompatibility properties of 316L stainless steel using SSP treatments alone without resorting to the use of pharmaceutical agents.

2. Materials and methods

2.1. Material and shot peening treatments

Mirror finish stainless steel grade AISI 316L sheets 10 mm thickness were supplied by Inoxea (IT). The chemical composition of the AISI 316L steel is reported in Table 1.

The 316L sheet was shot peened using two different sets of parameters: conventional shot peening (CSP) and severe shot peening (SSP); the latter set of parameters was chosen based on a numerical model previously developed by some of the authors [16] in a way to induce grain refinement on the surface layer of the material. Both shot peened series, after being peened using steel shots, were re-peened by glass beads for the purpose of decontamination from the residuals of the steel peening media.

The treatment parameters as well as the characteristics of the media used are presented in Table 2 and Table 3, respectively.

As-received (not peened, NP) substrates were used as controls in all of the experiments.

Following the shot peening treatment, the sheets were cut into small disks 10 mm in diameter using a water jet cutter. After each treatment, samples were divided into two batches: as-treated and ground. For the ground series, a very thin surface layer was removed from the shot peened surface and the as-received samples using Silicon carbide (SiC) 1200 and 2500 grit paper in order to remove the indentations generated on the treated surface to obtain identical surface roughness for all samples.

2.2. Surface mechanical and physical characterization

All samples were rinsed ultrasonically in acetone, ethanol and distilled water successively for 15 min each, to remove any kind of contaminant adhering to the substrate. They were then dried in an oven at 60 °C for 1 h before further analysis as described below.

Table 1
Chemical composition of AISI 316L stainless steel studied in this work (wt %).

Cr	Ni	Mo	Mn	Si	C	P	S	Nb	Cu	Co	N
17.11	10.15	2.03	1.34	0.47	0.022	0.034	0.001	0.009	0.41	0.26	0.049

Table 2
Aspects of the shot peening treatment.

Sample	Shot type	Almen intensity	Surface coverage%	Repeening	
				Shot type	Surface coverage
Not peened (NP)	–	–	–	–	–
Conventionally shot peened (CSP)	MI 230R	15A	100	AGB12	100%
Severely shot peened (SSP)	MI 230R	7C	1500	AGB12	100%

Table 3
Characteristics of the peening media (HRC is the Rockwell C hardness test scale used on hard materials>100 HRB).

Shot type	Material	Nominal diameter (μm)	Hardness (HRC)
MI 230R (Milgrandi spa, IT)	Cast steel	580	60
AGB12 (EisenwerkWürth Abrasives, DE)	Glass	120	47

2.2.1. Grain structure and size measurements

For microstructural evolution characterization, samples of each series were laterally sectioned, impregnated in a Phenolic hot mounting resin (Met Prep Ltd, UK), and ground with a series of SiC papers up to P4000 (average scratch size of 5 μm). Each section was further polished using polycrystalline diamond water-based suspensions with an average scratch size of 1 μm and 0.25 μm. For grain size measurements on NP and CSP samples, the top surface was subjected to the aforementioned polishing steps and etched by Beraha's reagent. All etched samples were then observed using a Leica DMLM light optical microscope in bright field mode. For NP and CSP samples, grain size measurements were performed by analyzing 140 grains from the top surface of 3 samples ($N = 3$) for each treatment type using ImageJ software (National Institute of Health, US) [17].

To measure the grain size of the SSP samples, XRD patterns of the samples were collected in a Philips X'Pert PW3020 diffractometer (Bragg Brentano parafocusing geometry) using a Cu kα ($\lambda = 1.54059$ Å) source over a 2θ range from 38° to 155°, scanned with a constant step size of 0.06° and time per step of 25 s. A reference sample of LaB6 (NIST standard) was used for instrumental broadening correction. The collected experimental spectra were then elaborated with the Rietveld method [18] by material analysis using diffraction (MAUD) software [19]. Line profile analysis was conducted to estimate the crystallite (domain) size. The anisotropic crystallite size was modeled using the Popa approach [20].

2.2.2. Surface morphology and roughness measurements

The surface morphology of the samples was observed using a Zeiss Evo MA 15 scanning electron microscope (SEM). An optical interferometric profilometer (WYKO NT 3300) was used to measure the surface roughness of the samples at the micrometer scale. Five measurements with a scan area of 2.43 × 1.85 mm^2 and 0.586 × 0.446 mm^2 were performed at random positions on 3 samples of each series for the as-treated samples and those ground after shot peening, respectively.

Nanometer scale surface roughness parameters were acquired with an NX-10 atomic force microscope (AFM, Park Systems, Suwon, Korea) using non-contact cantilever probes (PPP-NCHR, Park Systems). Topography data were collected at a scan size of 2 × 2 μm in a grid of 256 × 256 points. Also, in this case, five measurements were performed at random areas for each sample series. The most extensive standard surface roughness parameters (including: arithmetic mean (R_a), root mean square deviation (R_q), and peak to valley (PV) defined as the sum of the largest profile peak height and the largest profile valley depth within the sampling length according to ISO Standard 4287 [21]) were measured at different length scales using the aforementioned equipments.

2.2.3. Surface wettability measurements

Wettability was assessed through static deionized (DI) water contact angle measurements by the sessile drop method on a CAM 200 goniometer system (KSV Instruments) at ambient humidity and temperature. Using an auto-pipette system, multiple droplets with a uniform volume of 2 μL were deposited in various locations on the top surface of three samples from each sample series. The water contact angles were measured once the drop stopped spreading (after 5 s).

2.2.4. Residual stress measurements

The distribution of the residual stresses was assessed by XRD analysis using an AST X-Stress 3000 portable X-ray diffractometer (Cr Kα radiation, irradiated circular area of 2 mm diameter, $\sin^2(\psi)$ method, diffraction angle (2θ) of 128.8° corresponding to the lattice plane (2 2 0) scanned between −45° and 45°) with an exposure time of 20 s. At each step, a thin layer of material around 0.02–0.03 mm of thickness was removed by electro-polishing with a solution of acetic acid (94%) and perchloric acid (6%). After each electro-polishing step, the new thickness of the sample was measured with a Mitutoyo micrometer precision IDCH0530/0560. The FWHM (Full Width at Half the Maximum) intensity of the XRD peak was also extracted from the results.

2.2.5. Microhardness measurements

Lateral sections of the samples were prepared and polished for in-depth microhardness measurements to obtain a smooth surface relative to the indent scale. The tests were carried out using a Leica VMHT 30A microhardness tester equipped with a diamond Vickers indenter. The measurements were performed along three parallel paths starting from the treated surface towards the core material with a maximum force of 200 gf applied at a constant rate of 0.1 NS^{-1} with a dwell time of 15 s.

2.3. Cell assays

2.3.1. Cell culture

Primary human osteoblasts (fHObs, PromoCell, Heidelberg, Germany) were cultured in phenol-free osteoblast basal medium with osteoblast supplemental mix (PromoCell) and 1% penicillin/streptomycin in a 37 °C, humidified, 5% CO_2/95% air environment. Cells at passage numbers of 4–12 were used in these experiments.

2.3.2. Cell adhesion and proliferation

AISI 316L samples, treated as previously described, were cleaned

by sequential ultrasonication in acetone, 70% ethanol, and DI water for 30 min each. Samples were then placed individually into the wells of a 24-well plate and sterilized under UV light overnight. Before cell seeding, samples were rinsed twice with PBS to remove any possible debris. Osteoblasts were then seeded onto the samples at a density of approximately 20,000 cells/cm^2 and incubated under standard culture conditions for 4 h to determine cell adhesion. Cell proliferation was measured after 1, 3, and 5 days of culture. The media was changed on day 3 during proliferation trials. After the desired incubation time, each sample was rinsed with PBS and carefully transferred to a brand new plate. Then, fresh media was added to each well along with an MTS dye (Promega, Madison, WI) in a 5:1 ratio (media:MTS). Samples were incubated for 3 h to allow the MTS dye to completely react with the metabolic products of the adherent cells, and then 200 μL of the solution from each well was transferred to a 96-well plate in quadruplicate. The absorbance of the MTS solution was measured at a wavelength of 490 nm using a SpectraMax M3 microplate reader (Molecular Devices). Results were normalized by subtracting the absorbance values of blank wells containing samples without any cells from those values measured for the corresponding cell-seeded samples. The number of adherent cells was determined by comparing the resulting absorbance values to a standard curve constructed at the beginning of each trial.

2.3.3. Cell morphology and spreading

Osteoblasts (from a different donor) were seeded on the sterilized samples of both the as-treated and ground batches at a concentration of 15,000 cells/cm^2 and were cultured for up to 3 days. Following 24 and 72 h of culture, samples were fixed with a 4% paraformaldehyde (PFA) solution for 15 min at room temperature before permeabilizing the cells with a 0.1% Triton-X/0.1% Tween solution for 30 min at room temperature. Non-specific antigens were blocked with 5% goat serum for 30 min at room temperature. Cells were therefore incubated with the primary antibody solution (anti-vinculin, hVIN-1, Sigma, UK; 1:400) overnight at 4 °C for the detection of focal adhesion sites. The following day, the secondary antibody (AlexaFluor594, Life Technologies, UK; 1:500) was applied for 1 h at room temperature, preventing light exposure. Finally, cells were stained against phalloidin (AlexaFluor488, Life Technologies, UK; 1:40) for 30 min at room temperature and visualized with an inverted confocal laser scanning microscopy system (Leica DMIRE2, UK) by individually mounting the samples on cover glass bottom petri dishes with DAPI mounting medium (Life Technologies, UK).

In order to quantify the cell area and the formation of focal adhesions (expressed as the percentage of vinculin expression over the cell area) as a function of the grain size (ground batch), 40 individual cells were averaged from two independent experiments after 1 day of culture. ImageJ software [17] was used to finally process the images.

Cell morphology was further investigated using SEM. After 24 h of culture, cells were fixed with 2.5% glutaraldehyde (Sigma, UK) in PBS for 30 min at 4 °C and dehydrated with a graded ethanol series (50%, 70%, 90%, and 100%). Samples were finally washed with hexamethyldisilazane (HMDS; Alfa Aesar, US), air-dried in a fume hood and gold sputtered for SEM analysis. Images were acquired at 500x magnification using a Zeiss Evo MA 15 SEM with an accelerating voltage of 15 kV.

2.4. Bacteria assays

2.4.1. Bacteria culture

A single isolated bacterial colony was removed from its starter plate and inoculated into 4 mL of nutrient medium. 30 g/L tryptic soy broth (TSB) was used to culture *S. aureus* (*S. aureus*, ATCC 12600), *S. epidermidis* (*S. epidermidis*, ATCC 35984), and *Pseudamonas aeruginosa* (*P. aeruginosa*, ATCC 27853). Ampicillin-resistant *E. coli* (Amp-R *E. coli*, HB101 K-12, Bio-Rad, Hercules, CA) were cultured in 25 g/L Luria broth (LB). Inoculated colonies were cultured to late exponential phase (~16 h) in a shaking incubator at 37 °C, and then diluted in their respective media to achieve an optical density of 1.0 at a wavelength of 600 nm (~10^9 cells/mL). Spectraphotometrically measured cell densities were verified by performing colony forming unit assays for each bacterial species used. Bacteria solutions were then diluted 1:1000 in 3 g/L TSB (2.5 g/L LB for *E. coli*) to a density of 10^6 cells/mL for seeding onto samples.

2.4.2. Bacteria adhesion and growth assays

Cleaned and sterilized 316L samples were placed individually into the wells of a 24-well plate and rinsed twice with PBS. 2 mL of the prepared bacteria suspensions (10^6 cells/mL) were then pipetted onto each sample and the plates were placed into a stationary incubator maintained at 37 °C and 5% CO_2/95% air. After 24 or 48 h of incubation, the samples were rinsed three times with PBS and then placed into 10 mL of PBS to be vortexed for 40 s, thereby releasing the attached bacteria from each sample into the surrounding PBS. This stock was then diluted 1:10 and 1:100 in PBS and each dilution was pipetted onto 30 g/L TSB agar plates (5 x 10 μL spots per dilution). Colony forming units (CFU) were then counted manually after ~14 h of incubation. The media was changed after 24 h for samples undergoing 48 h of incubation.

2.4.3. Live/dead fluorescent microscopy assays

Samples were prepared and seeded with bacteria solutions as described above. After 24 h of incubation, the samples were rinsed three times with PBS and then stained for fluorescence microscopy analysis. The Live/Dead Baclight bacterial viability kit (Life Technologies) was used to view adherent bacteria. Equal volumes of 3.34 mM SYTO 9 dye and 20 mM propidium iodide were mixed together and then added to DI water at 2.5 μL per mL of water. 2 mL of this solution was added onto each sample and allowed to incubate in the dark for 15 min. Following this short incubation, the samples were flipped upside down into a new 24-well plate containing 1 mL of DI water per well and viewed under a 10x objective using a Zeiss Confocal LSM 700 microscope.

2.4.4. Statistical analysis

For all cell and bacteria cultures, the reported arithmetic means and standard deviations refer to averages of three independent experiments, using three replicates per each group. The analysis of variance (ANOVA) method, followed by a Bonferroni's post-hoc test, was used to determine statistical significance.

3. Results

3.1. Substrate microstructure

Fig. 2 (a)-(c) show the microstructure of the sample sections etched after grinding a thin top surface layer. It can be observed that shot peening activated different deformation mechanisms in the material which promoted strain hardening as well as grain refinement. In the layer just under the shot peened surface (Fig. 2 (b) and (c)), the presence of multiple slip bands constructed a network pattern in the heavily deformed grains indicating dislocation accumulation. The slip bands were parallel/perpendicular within each grain, and were oriented at different angles from those in the adjacent grains. The thickness of the affected layer was measured to be around 150 μm and 300 μm for CSP and SSP samples, respectively, excluding the thickness of the deformed layer

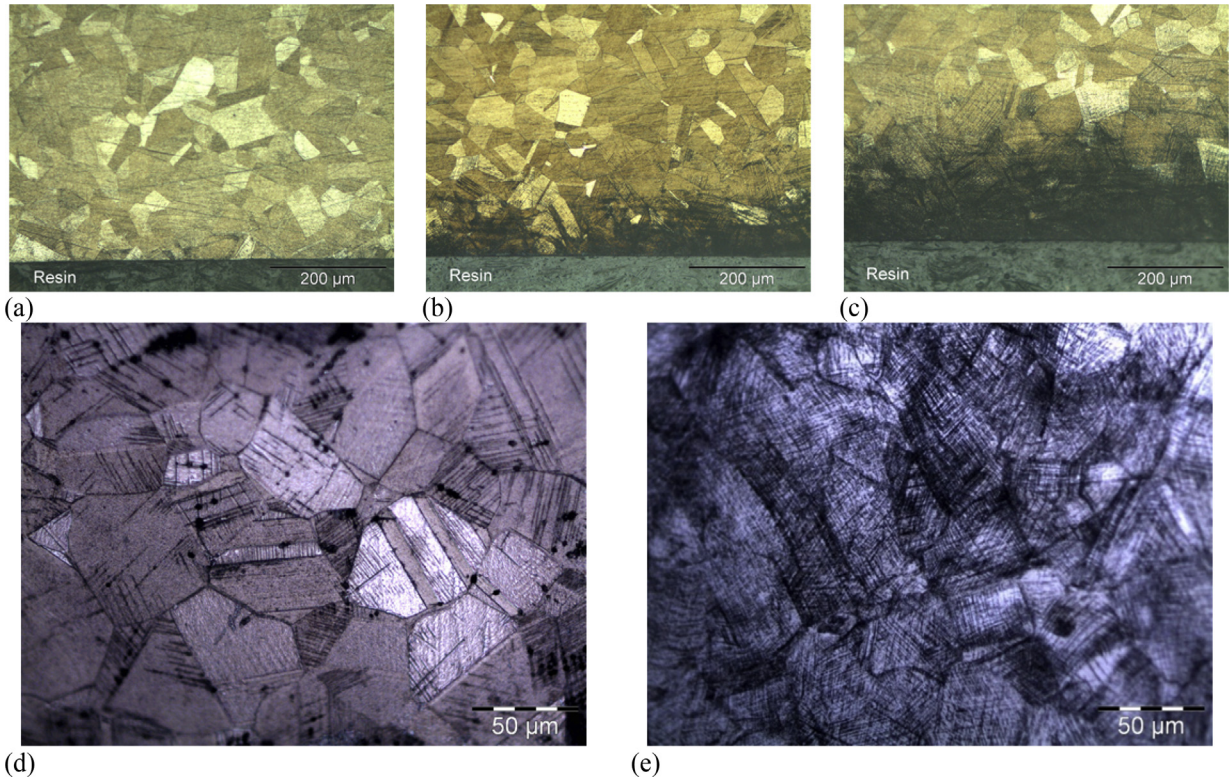

Fig. 2. Cross section optical micrographs showing the microstructure of (a) NP, (b) CSP, and (c) SSP samples etched by Beraha's reagent. Representative optical microscopy images of the top surface layer of (d) NP, (e) CSP samples after etching. NP = not peened; CSP = conventionally shot peened; and SSP = severely shot peened.

removed via grinding. Deformation twinning was also observed in the optical micrographs of all samples including NP series (Fig. 2 (a)); thus it is postulated that they are mainly attributed to the cold working and annealing of the as-received material. After etching, the difference in atomic configurations induced different colors at each side of the twin boundary, defined as a planar interface for which the arrangement of atoms on the two sides are mirror reflections of each other. Similar deformation mechanisms (as observed in Fig. 2 (a)-(c)) have been reported elsewhere for 316L SS using other SPD methods [22,23].

Going more in depth, with a reduced applied strain and strain rate, the density of slips decreased and the dense irregular multiple-slips were gradually replaced by random single ones. That is why the grain boundaries cannot be identified through optical microscopy in the layer just under the treated surface for the SSP samples. The grain structure then became clear moving further into the material. Accordingly, different techniques were adopted for grain size measurements in different samples. For NP and CSP series, the measurements were performed by analyzing optical microscopy images of the topmost surface layer of the material after etching (Fig. 2 (d) and (e)). The results are presented in Table 4.

The crystallite size for the surface layer of the SSP treated samples was extracted from the XRD patterns collected within the range of 38°−155° using line profile analysis, and was estimated to be 25 nm. This grain size was averaged through the penetration depth of the X-ray which in turn depends on the mass absorption coefficient of the sample to the radiation and the incident angle of the X-ray beam [24]. Considering the mass absorption data was for CuK alpha, the penetration depth for 50% intensity was calculated to be 1.41 μm for the SSP samples.

Table 4
Average grain size measurements on the top surface layer of NP, CSP, and SSP samples.

Sample	NP	CSP	SSP
Average grain size	63 ± 5 (μm)	44 ± 4 (μm)	25 ± 5 (nm)

3.2. Surface morphology and roughness

The top view SEM observations, Fig. 3 (a)–(c), represent the expected smooth surface for the NP samples, while the effect of shot peening towards increasing the surface roughness and creating multiple overlapping indentations can be clearly observed for the CSP and SSP samples. A similar top surface morphology was observed for CSP and SSP samples, with a slightly more chaotic texture and a higher number of micro defects and craters for the SSP samples. However, measurements performed by interferometric profilometry and AFM at lower magnifications revealed different surface topographies and multiple peaks and valleys on the treated surfaces induced by different shot peening parameters. The average standard surface roughness parameters measured by interferom-etry are presented in Table 5, where the roughness parameters for the shot peened samples followed a reasonable trend as it is well-established that increasing the Almen intensity and surface coverage during the shot peening process increases surface micro-roughness [25]. For the samples that were slightly ground after shot peening, no significant difference was observed for the surface roughness of the different substrates, as expected.

Considering that standard surface roughness parameters are scale dependent, the interferometry profilometer was used with much larger scan lengths compared to the AFM and consequently can provide more data about the microsurface roughness of the specimens. AFM topographical images (scan areas of 2 × 2 μm) representative of each sample group are presented in Fig. 3 (d)-(f), and the standard surface roughness parameters are compared in

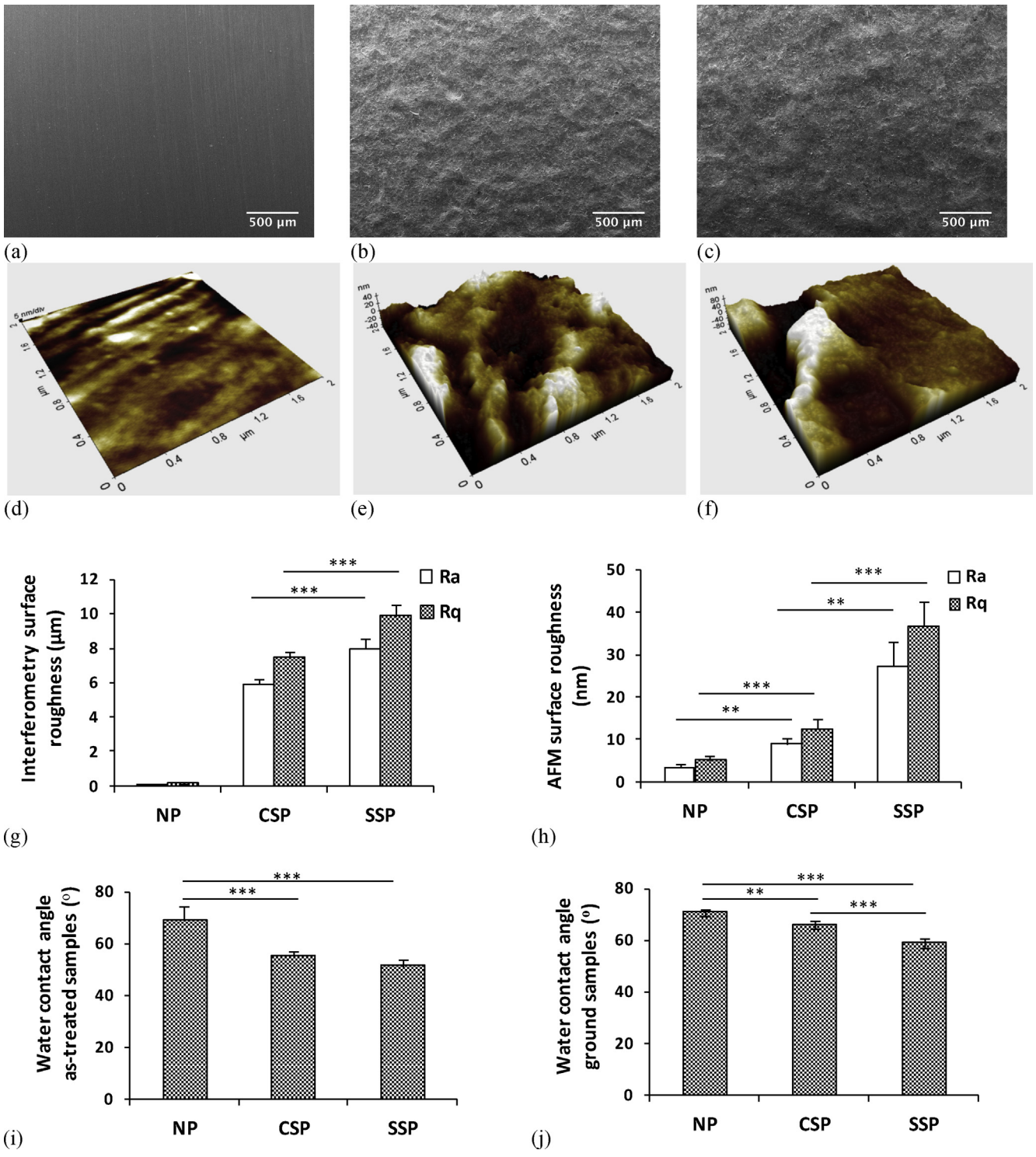

Fig. 3. Top surface scanning electron micrographs of (a) NP, (b) CSP, and (c) SSP samples; atomic force microscope topographical images of (d) NP, (e) CSP, and (f) SSP samples; (g) microscale surface roughness parameters measured by optical interferometric profilometry on an area of 2.43 × 1.85 mm^2; (h) nanoscale surface roughness parameters measured by AFM on an area of 2 × 2 µm; static water contact angles measured on the surfaces of (i) as-treated samples and (j) ground samples (DI water droplets of 2 µL). NP = not peened; CSP = conventionally shot peened; SSP = severely shot peened. R_a = arithmetic mean, and R_q = root mean square (rms) surface roughness. Data = mean ± St. Dev; $N = 3$, $^{**}p < 0.05$, $^{***}p < 0.005$.

Fig. 3 (h), demonstrating that nanoscale surface roughness also increased with SSP treatment.

3.3. Substrate wettability

The extent of the surface wettability can directly mediate the absorption of proteins to the implant surface and therefore affect cell adhesion and its functions at the implant–tissue interface. Surface topography and refined grain structure are two parameters that can affect the surface contact area as well as surface energy, and consequently promote the interaction of the substrate with the wetting media. In case of as-treated series, all sample surfaces were

Table 5
Surface roughness of the samples measured by interferometry.

Treatment	R_a (μm)	R_q (μm)	PV (μm)
NP	0.09 ± 0.02	0.13 ± 0.02	6.31 ± 2.90
CSP	5.92 ± 0.29	7.43 ± 0.38	52.84 ± 4.58
SSP	8.14 ± 0.63	10.10 ± 0.76	63.43 ± 3.27
NP-ground	0.031 ± 0.08	0.039 ± 0.01	0.19 ± 0.06
CSP-ground	0.029 ± 0.09	0.036 ± 0.01	0.19 ± 0.07
SSP-ground	0.031 ± 0.09	0.038 ± 0.01	0.22 ± 0.09

found to be slightly hydrophilic through water contact angle measurements, with increased wettability observed as the Almen intensity increased (Fig. 3 (i)). That is, the highest wettability was measured on SSP treated samples. The surface of the ground samples demonstrated the positive effect of grain refinement in enhancing surface wettability (Fig. 3 (j)).

3.4. Residual stress measurements

The average in-plane distribution of residual stresses and the FWHM parameter for the as-received, CSP and SSP samples are respectively shown in Fig. 4 (a), and (b) as a function of distance from the treated surface. The profiles showed much deeper compressive stresses for the SSP samples. The FWHM profile, shown in Fig. 4 (b), indicates the effect of shot peening in all cases to induce surface work hardening, while a higher increase was observed for the SSP treatment compared to CSP. In the case of the CSP samples, the FWHM values tended to reach the values of the core material much faster compared to the SSP samples.

3.5. Microhardness measurements

The microhardness profile with corresponding depth for all samples is presented in Fig. 4 (c). The effect of the surface treatments on increasing the microhardness is evident, following the same trend demonstrated for the FWHM showing maximum values at the surface gradually decreasing to reach the as-received mate-rial microhardness. As it can be observed in Fig. 4 (b), deeper than almost 0.6 mm, no appreciable difference was observed between the samples, indicating that this was the maximum depth affected by the treatments.

3.6. Cell proliferation

The shot peening treatments did not have a significant effect on the proliferation of osteoblasts on 316L (Fig. 5 (a) and (b)). Although SSP samples supported increased osteoblast densities after 1 day of culture, presumably due to the increased surface wettability or surface area, cell densities were found to be equivalent between all samples after 5 days. Thus, compared to the as-received 316L, SSP treated samples maintained a similar early stage growth rate for osteoblasts.

3.7. Cell morphology and spreading

Osteoblasts were cultured up to 3 days and stained against actin and vinculin to initially study the cell cytoskeleton structure and the formation of focal adhesions, on the as-treated substrates. As shown in Fig. 5 (c)-(e), osteoblasts presented a well-defined

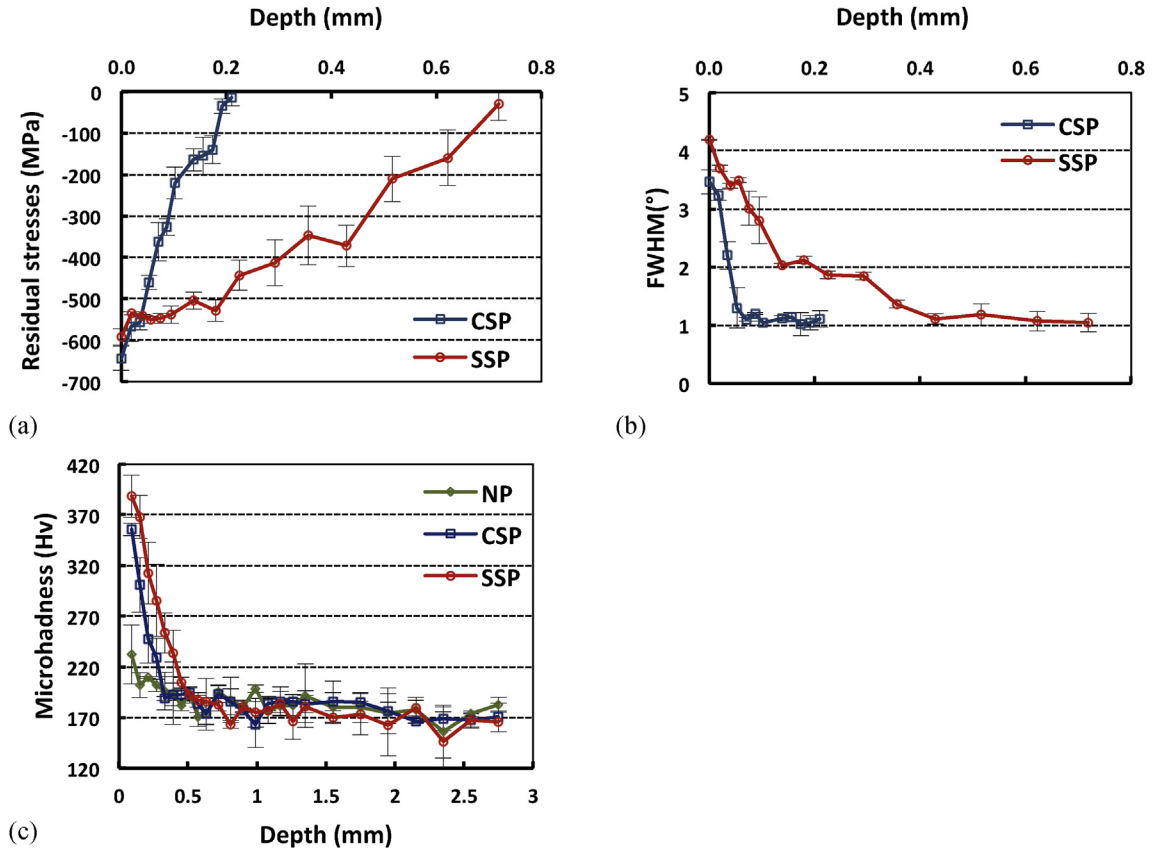

Fig. 4. In-depth distribution of (a) residual stresses, (b) FWHM in different samples measured by a portable X-ray diffractometer (a thin layer of material was electrochemically removed for each measurement to minimize alteration of residual stresses), and (c) microhardness profile measured from the treated surface towards the core material. The data are the average of three measurements at each depth. NP = not peened; CSP = conventionally shot peened; SSP = severely shot peened; FWHM = full width at half the maximum; Data = mean ± St. Dev; $N = 3$.

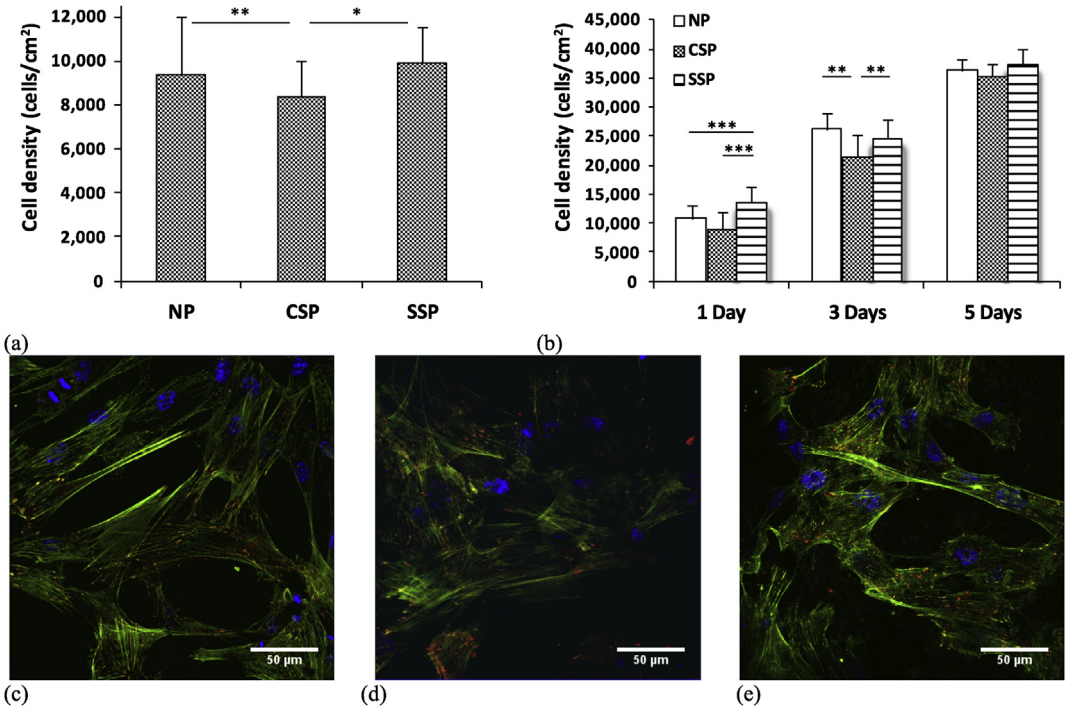

Fig. 5. (a) Adhesion of osteoblasts 4 h after seeding, and (b) Proliferation of osteoblasts after 1, 3 and 5 days of culture as measured by an MTS assay (Data = mean ± St. Dev; $N = 3$, $^{*}p < 0.05$, $^{**}p < 0.01$, $^{***}p < 0.001$. Cell densities for the same samples at different time points were all statistically different ($p < 0.01$)). Fluorescence micrographs of osteoblasts cultured on as-treated samples after 3 days of culture on (c) NP, (d) CSP, and (e) SSP samples. (Phalloidin488, AlexaFluor594 and DAPI respectively stained actin cytoskeleton (green), vinculin focal adhesion contacts (red) and cell nuclei (blue)). (For interpretation of the references to color in this figure legend, the reader is referred to the web version of this article.)

cytoskeleton arrangement as evidenced by the presence of actin-stress fibers and vinculin-containing focal-adhesions indicative of a high degree of attachment to all as-treated surfaces. In compar-ison to the more elongated osteoblasts on as-received samples (Fig. 5 (c)), cells on shot peened substrates (Fig. 5 (d) and (e)) appear to acquire a predominantly polygonal shape with increased num-ber of focal adhesions.

As previously demonstrated by interferometer measurements (Table 5), following grinding, the surface roughness of samples was reduced to have equivalent surface topography for all series. As a consequence, it was possible to evaluate the sole effect of grain size on cell attachment. The results of the experiments on ground samples revealed that osteoblast response to the metal substrates was improved as a function of grain size. After 1 day of culture, osteoblasts on shot peened ground surfaces (Fig. 6 (b) and (c)) presented mature focal adhesions and increased cell spreading compared to cells on as-received surfaces (Fig. 6 (a)). Results were confirmed by SEM observations (Fig. 6 (d)–(f)).

To better highlight differences between samples in terms of osteoblast spreading and focal adhesion formation, individual cells were analyzed and data are presented in Fig. 6 (g) and (h). Compared to the as-received surfaces, grain refinement allowed for better cell spreading ($^{*}p < 0.05$), which was followed by an increase in vinculin expression ($^{***}p < 0.001$), normalized per cell area.

3.8. Bacterial adhesion and growth

Shot peening treatments significantly decreased the attachment and growth of the gram-positive species *S. aureus* and *S. epidermidis* after 1 day of culture (Fig. 7 (a) and (c)). Specifically, the number of colony forming units (CFU) for these species decreased as the sample surface roughness increased. Representative fluorescence micrographs of this result are shown for *S. epidermidis* in Fig. 7 (i)-(k). Gram-positive bacterial adhesion was less affected after 2 days of culture, although *S. aureus* growth was significantly stunted on SSP samples.

Alternatively, shot peening treatments did not affect the adhesion of the gram-negative species *P. aeruginosa* or Amp-R *E. coli* (Fig. 7 (e) and (g)). For all bacterial species tested, shot peening treatments followed by surface grinding did not significantly affect bacterial attachment and growth, with the exception of *S. epidermidis* at 2 days, *P. aeruginosa* at 1 day, and Amp-R *E. coli* at 2 days (Fig. 7 (d), (f), and (h), respectively). This result indicates that the sample surface roughness, and not grain size, directly affects gram-positive bacterial attachment and growth.

4. Discussion

Mechanical cues in the cell and bacteria microenvironment provide signals that can modulate their phenotype, gene expression, and functions. In this regard, various micro- and nano-fabricated platforms have been devised to control the biological interface through surface topography, grain structure, rigidity, mechanical strain, shear stress, etc. [8,26,27]. In the present study, SSP, a mechanical surface treatment that is based on plastic deformation, was used to induce hierarchical surface roughness as well as surface grain refinement down to the nanoscale on the top surface layer of 316L SS samples. Compared to other treatments that induce grain refinement through plastic deformation such as surface mechanical attrition treatment (SMAT), high pressure torsion (HPT), equal channel angular pressing (ECAP), SSP is less demanding and more adaptable in inducing grain refinement. It is applicable to a wider range of metallic materials without involving geometrical and dimensional restrictions, contrary to most of the aforementioned techniques [11]. In addition, SSP markedly increases surface roughness, resulting in enhanced total surface area

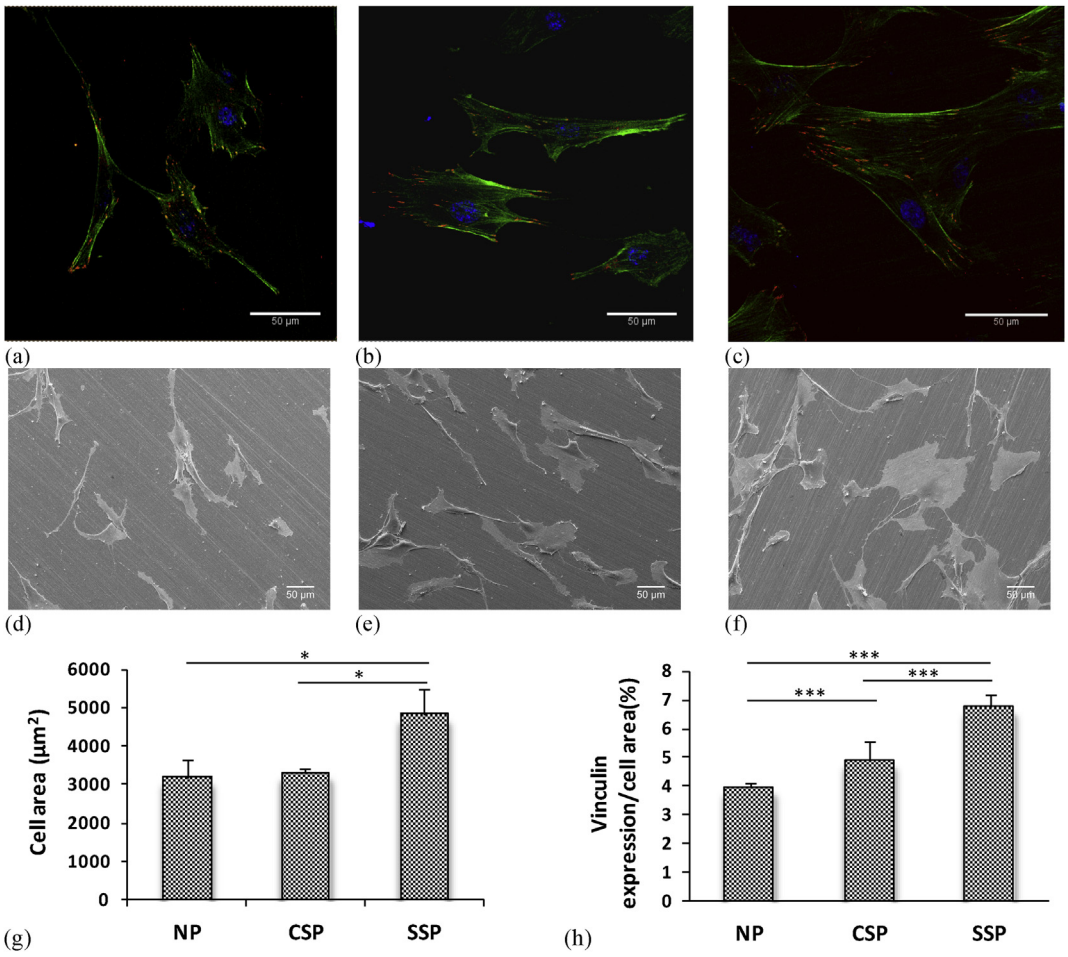

Fig. 6. Fluorescence micrographs of osteoblasts cultured on the shot peened and successively ground sample surfaces after 1 day of culture on (a) NP, (b) CSP, and (c) SSP samples. (Phalloidin488, AlexaFluor594 and DAPI stained actin cytoskeleton (green), vinculin focal adhesion contacts (red) and cell nuclei (blue), respectively). Scanning electron micrographs of osteoblasts cultured for 1 day on shot peened and successively ground (d) NP, (e) CSP, and (f) SSP samples. (g) Cell area and (h) vinculin expression evaluated for 40 individual cells from two independent experiments after 1 day of culture; error bars represent standard deviation. Data = mean ± St. Dev; $N = 3$, $^{*}p < 0.05$, $^{***}p < 0.001$. (For interpretation of the references to color in this figure legend, the reader is referred to the web version of this article.)

and superior mechanical anchorage.

The treated 316L SS samples were used to evaluate the effect of SSP on cell and bacteria short term responses, and a second grinding step was employed to separate the effects of surface topography from grain size. Microstructural characterization after SSP indicated that the proposed treatment induced surface grain refinement down to an average grain size of 25 nm on the top surface layer of 316L SS samples, as measured by XRD (Table 4). Morphological observations by SEM (Fig. 3 (a)-(c)) and interferometric roughness measurements (Table 5) indicated irregular surface topography with a more chaotic texture and higher standard roughness parameters at the microscale, generated by multiple overlapping indentations after the SSP treatment. AFM measurements (Fig. 3 (d)-(f)) confirmed a hierarchical surface topography and the presence of nano-rough surface features with a similar trend to the evolution of micro-roughness, such that the highest surface roughness parameters were measured on the SSP samples both at the micro and nanoscale (Fig. 3 (g) and (h)). Surface wettability measurements also showed higher surface hydrophilicity for the SSP samples compared to CSP and the as-received material (Fig. 3(i)). Surface wettability is affected both by surface features and grain size. Therefore, to separate the effect of these two parameters, a series of samples were slightly ground to remove the surface indentations generated by the impacts and obtain identical surface roughness for all samples including the as-received series (Table 5). The wettability profile of the samples after surface grinding also followed the same trend, presenting higher surface wettability for the SSP-ground samples, thus, confirming the direct effect of grain size on hydrophilicity (Fig. 3(j)).

Residual stress and microhardness measurements were carried out to characterize the variations in mechanical properties induced by the peening processes. The results revealed the notable effect of SSP treatment in creating a deep work hardened surface layer with high compressive residual stresses (Fig. 4). These effects will promote the mechanical strength of the material particularly under cyclic loading by inhibiting both fatigue crack initiation and propagation rates. The presence of nanograins at the top surface layer increases the fatigue crack initiation threshold whereas the microcrystalline interior acts effectively in deflecting the crack growth path by grain boundaries and thus reducing the growth rate [13,14]. These properties generally increase the performance and durability of load-bearing orthopedic implants.

Primary human osteoblasts were seeded onto the treated samples to examine the effect of surface topography on cell adhesion and proliferation for up to 5 days (Fig. 5 (a) and (b)). Osteoblasts were shown to adhere and grow at roughly the same rate on all three series of samples (NP, CSP, and SSP), indicating that the SSP treatments did not significantly affect the early stage growth of

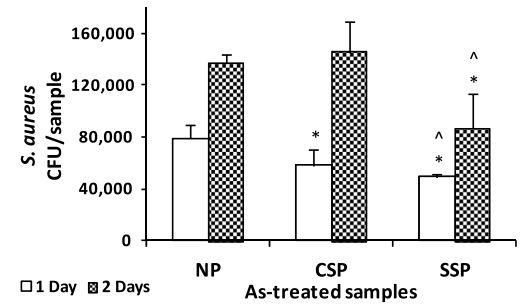

(a)

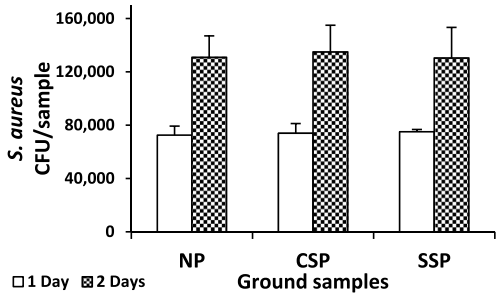

(b)

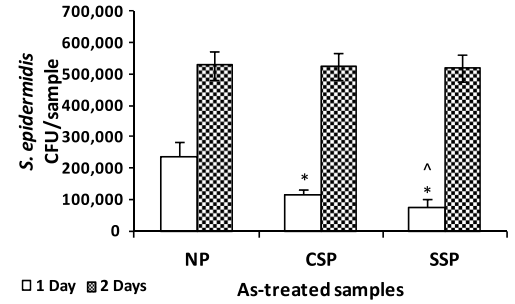

(c)

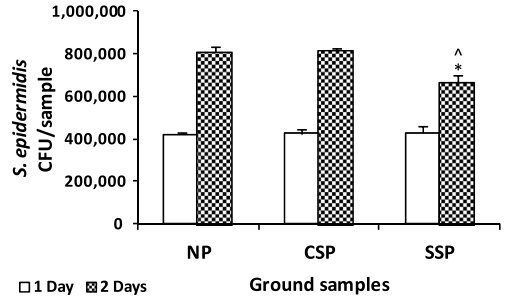

(d)

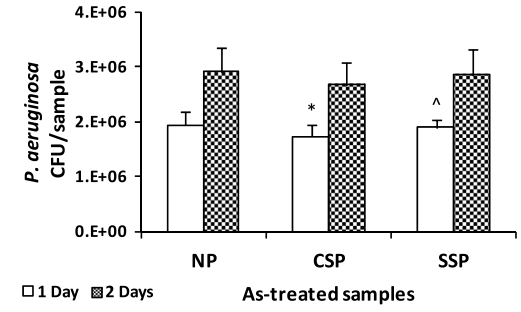

(e)

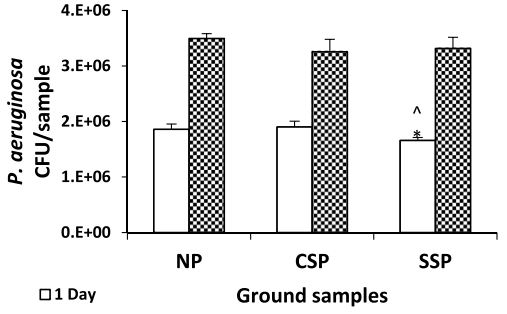

(f)

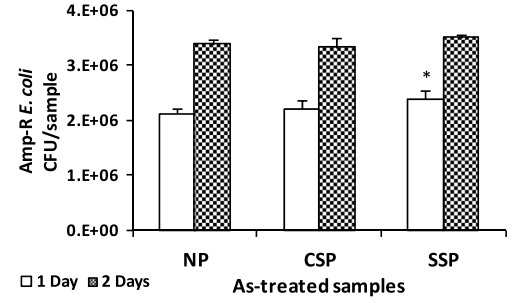

(g)

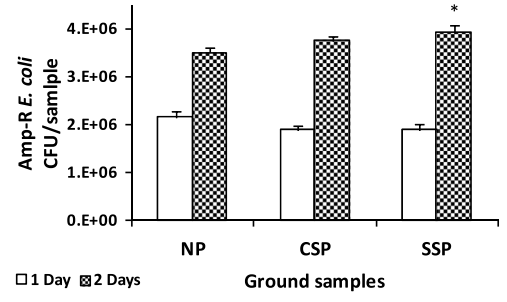

(h)

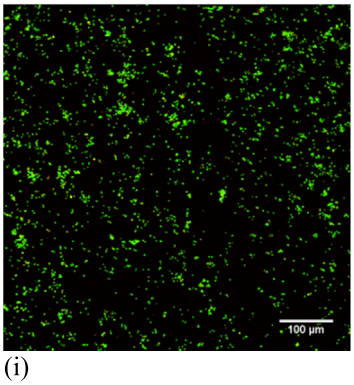

(i)

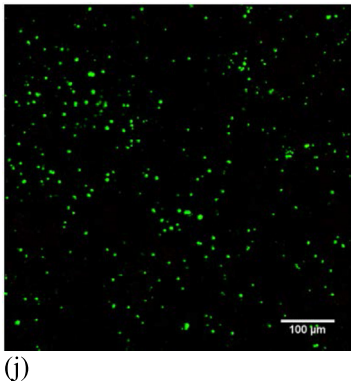

(j)

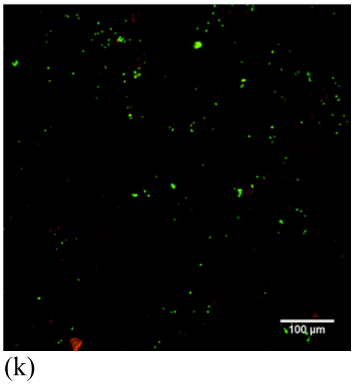

(k)

osteoblasts. This result contributes to the already indefinite findings, as several researchers have reported increased adhesion and proliferation of osteoblasts on nano-rough compared to conventional materials [28,29], whereas many others have found no significant correlation [30,31]. As reported by Bigerelle et al., it is possible that the so-called "process effect" (the specific morphology of surface features induced by different material processing techniques) plays a larger role in determining cell functions than simply the roughness amplitude ("roughness effect") which is the most often reported characterization of roughness [32]. In fact, conventional roughness parameters are not able to fully describe the surface features and additional roughness parameters should be considered to provide a more precise description of the morphological aspects of surfaces including the formation of irregularities and their spatial distribution. Further study is needed to test this theory.

Cell membrane characteristics and cell dimensions can also affect their response to the surface features of the substrate. The mem-brane fluidity and the larger size of osteoblasts compared to surface nanofeatures can impair them from detecting these features, as previously demonstrated for nanocolumnar coating interactions with osteoblasts where the anchoring elements of the cells were not found to be sensitive to the substrate nanofeatures [31].

Although osteoblast growth for up to 5 days was minimally affected by SSP treatments, positive changes in other measures of cellular activity were observed. Cell cytoskeleton structure and the formation of focal adhesions were studied respectively for shot peened samples and those surfaces ground after shot peening using both fluorescence microscopy (Fig. 5 (c)-(e) and Fig. 6 (a)-(c)) and SEM (Fig. 6 (d)-(f)). Slight morphological differences were observed between the cells seeded on shot peened (CSP and SSP) substrates compared to the as-received samples, showing predominantly polygonal cell shapes on the shot peened series. However, comparison of the early interaction of osteoblast cells with the shot peened and successively surface ground samples with the as-received material suggests positive effect of reduced grain size on cell spreading, development of actin stress fibers, and expression of focal adhesions (Fig. 6 (a)-(c)). The outspread morphologies and higher vinculin expression was quantitatively assessed on SSP-ground samples, and confirmed the beneficial effect of grain refinement. Thus, although no differences in osteoblast proliferation were observed on the differently treated samples, select protein expressions were improved on samples exhibiting higher hydrophilicity, possibly because these surfaces offer more active sites for cell anchoring proteins [5]. Additionally, reduced cellular proliferation together with increased protein expression often indicates increases in later stage cell activities such as differentiation and mineralization [33,34]. Further analysis into osteoblast differentiation and maturation are needed to verify this hypothesis on the present samples.

Regardless, all samples provided comparable but good adhesion and proliferation for osteoblasts; thus, the SSP treatment did not interfere with the early stages of osteoblast cell growth and maintained the biocompatibility of the as-received material.

Bacterial infection is among the most common and challenging post-surgical complications affecting biomedical implants. Specifically, the gram-positive strains *S. aureus* and *S. epidermidis* are especially dangerous as they account for roughly two-thirds of orthopedic infections [35]. Here, the SSP treatment was shown to significantly decrease the adhesion of *S. aureus* and *S. epidermidis* onto 316L SS. This effect was attributed singularly to the increased surface roughness of shot peened samples, as the SSP-ground samples (exhibiting a smaller average grain size but no differ-ences in surface roughness) did not cause changes in bacterial adhesion compared to NP-ground or CSP-ground samples. To our best knowledge, this is the first time that the effects of surface roughness and grain size on bacterial adhesion have been separated. Contrary to the osteoblasts results, the bacteria have a smaller size, a more rigid membrane, and a more stable characteristic shape relative to eukaryotic cells. There are multiple reports on the significant role of various surface irregularities, comparable to the size of the bacteria, on their adhesion and subsequent functions [7,31]. The high surface density of nano-irregularities seems to limit the number of anchoring points for these bacteria, reducing the surface area in contact with their membrane. This reduced area impairs the adhesion of gram-positive bacteria.

Interestingly, neither increasing surface roughness nor decreasing grain size had any significant effect on the adhesion or growth of the gram-negative bacteria *P. aeruginosa* or amp-R *E. coli*. We hypothesize that gram-negative bacteria do not experience adhesion inhibition on these surfaces with increased nanoroughness because they possess an extra outer membrane surrounding their peptidoglycan layer which gram-positive bacteria do not possess [36]. This outer membrane is more fluidic (similar to mammalian cell membranes) and thus may allow the gram-negative bacteria a more cushioned interaction with their substrate compared to the rigid peptidoglycan layer of gram-positive bacteria, effectively buffering them from the antibacterial effects of high nanoscale surface roughness.

It is also interesting to note that, with a couple of exceptions, bacteria of the same strain were found on the differently treated samples in roughly equivalent numbers after 2 days of culture. Thus, it appears that SSP treated samples satisfactorily inhibited the first phase of bacterial attachment (physicochemical in nature), but were unable to modify long term bacterial colonization [35]. However, the antibacterial properties exhibited here by SSP treated samples against *Staphylococcus* strains (the most prevalent in orthopedics by far) could be crucial *in vivo* by inhibiting early stage bacterial adhesion and, thus, allowing the body to more easily clear the infection.

Overall, the density of gram-positive bacteria (*S. aureus* and *S. epidermidis*) after 1 day of culture was inversely proportional to rms surface roughness, and osteoblast expression of vinculin focal adhesions was inversely related to the water contact angle on ground samples (which was directly related to grain size refinement) (Fig. 8). Relationships were not found between vinculin expression and surface roughness, or between bacterial attachment and surface hydrophilicity.

The results presented here indicate that a complex set of parameters including surface topography, grain size, as well as cell and bacteria characteristics are involved in the interactions of cells and bacteria with the SSP treated substrates. Differences in cell and bacteria adhesion and interactions with the substrate topography may be attributed to their size range (osteoblasts 10−50 μm and bacteria about 1 μm in diameter) and how their membranes respond to the surface state of the substrate. Cellular responses to

Fig. 7. (a)−(h) Adhesion of four different bacteria strains onto as-treated and ground samples following 1 and 2 days of incubation (data represents mean ± St. Dev; $N = 3$; $^{*}p < 0.01$ compared to NP at the same time point; $^{\hat{}}p < 0.01$ compared to CSP at the same time point. CFU/sample counts were statistically higher ($p < 0.01$) when cultured for 2 days compared to 1 day for all samples. Representative fluorescent micrographs of *Staphylococcus epidermidis* cultured for one day on (i) NP, (j) CSP, and (k) SSP as-treated samples (SYTO® 9 and propidium iodide respectively stained live (green) and dead (red) bacteria cells); error bars represent standard deviation, CFU = colony forming units. (For interpretation of the references to color in this figure legend, the reader is referred to the web version of this article.)

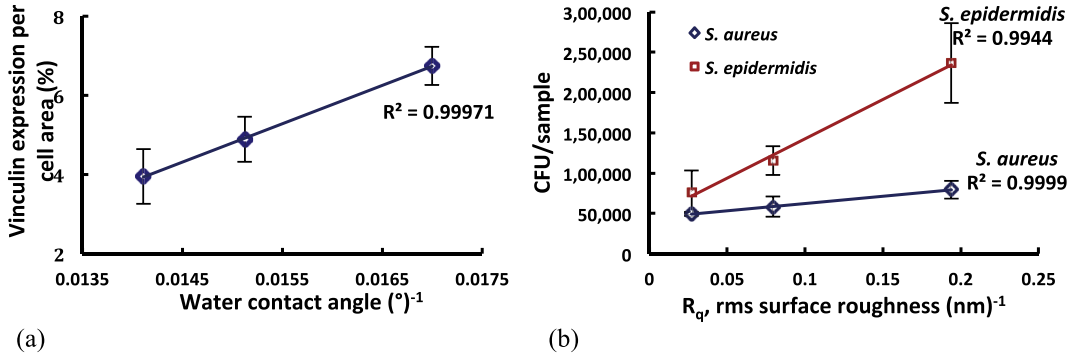

Fig. 8. Separating the effects of surface roughness and wettability on biological interactions. Osteoblast vinculin expression was directly proportional to the reciprocal of the water contact angle on ground samples (a), whereas bacterial adhesion after 1 day was directly proportional to the reciprocal of the root mean square (rms) surface roughness (b). Error bars represent St. Dev.

the topographical and structural aspects of the substrate material are reported by some studies in the literature to be cell-type dependant [37–39], and our results confirmed this dependency, specifically for bacteria. Cell spreading was found to be directly affected by grain size, and consequently by hydrophilicity. Osteoblast proliferation and gram-negative bacteria (*P. aeruginosa* and amp-R *E. coli*) adhesion and growth showed little sensitivity to grain size and topographical features here, whereas gram-positive bacteria (*S. aureus* and *S. epidermidis*) adhesion and growth was notably manipulated by the surface topography and not by the grain size.

5. Conclusion

Simultaneous induction of hierarchical surface roughness, surface grain refinement down to the nano-regime, and enhanced mechanical properties through severe shot peening treatment provide extended functionality to the treated material for orthopedic implants. The results of the present study indicate enhanced mechanical properties, maintained cell functions and reduced gram-positive bacteria adhesion on severe shot peened 316L stainless steel. Decreased activity of the most prevalent gram-positive bacteria in orthopedics can result in reducing the risk of infections and consequent long-term implant-related complications and allow for subsequent tissue integration without using antibiotics. The enhanced mechanical properties also promote efficiency in stabilizing the bone segments and performing well under relatively large amplitudes of static and dynamic loading.

The proposed approach is promising for production of multi-functional orthopedic implants and should be further studied for improving efficiency in reducing late complications, patient discomfort, and healthcare costs.

Acknowledgments

The authors declare no conflict of interests in this work. SB acknowledges funding from the Faculty For The Future Program (Schlumberger Foundation), MIT-Italy program (Progetto Rocca) and the Politecnico di Milano International Fellowship (PIF). DJH acknowledges funding from NSF-IGERT Grant No. 0965843, and thanks Ms. Divya Muthusamy for her help in the lab. VNM, ACdL and AEM acknowledge funding from the European Research Council (Grant No. 240446). The authors would like to thank Metal Improvement Company (MIC) for support on surface treatments.

References

[1] T.J. Webster, C. Ergun, R.H. Doremus, R.W. Siegel, R. Bizios, Enhanced functions of osteoblasts on nanophase ceramics, Biomaterials 21 (2000) 1803–1810.
[2] M. Nikkhah, F. Edalat, S. Manoucheri, A. Khademhosseini, Engineering microscale topographies to control the cell–substrate interface, Biomaterials 33 (2012) 5230–5246.
[3] S. Bagherifard, R. Ghelichi, A. Khademhosseini, M. Guagliano, Cell response to nanocrystallized metallic substrates obtained through severe plastic deformation, ACS Appl. Mater Interfaces 6 (2014) 7963–7985.
[4] M. Guvendiren, J.A. Burdick, Stiffening hydrogels to probe short- and long-term cellular responses to dynamic mechanics, Nat. Commun. 3 (2012) 792.
[5] A. Dolatshahi-Pirouz, T. Jensen, D.C. Kraft, M. Foss, P. Kingshott, J.L. Hansen, et al., Fibronectin adsorption, cell adhesion, and proliferation on nanostructured tantalum surfaces, ACS Nano 4 (2010) 2874–2882.
[6] A. Dolatshahi-Pirouz, M. Nikkhah, K. Kolind, M.R. Dokmeci, A. Khademhosseini, Micro-and nanoengineering approaches to control stem cell-biomaterial interactions, J. Funct. Biomater. 2 (2011) 88–106.
[7] S.D. Puckett, E. Taylor, T. Raimondo, T.J. Webster, The relationship between the nanostructure of titanium surfaces and bacterial attachment, Biomaterials 31 (2010) 706–713.
[8] A.K. Epstein, A.I. Hochbaum, P. Kim, J. Aizenberg, Control of bacterial biofilm growth on surfaces by nanostructural mechanics and geometry, Nanotechnology 22 (2011) 494007.
[9] R.Z. Valiev, R.K. Islamgaliev, I.V. Alexandrov, Bulk nanostructured materials from severe plastic deformation, Prog. Mater. Sci. 45 (2000) 103–189.
[10] R. Valiev, Nanostructuring of metals by severe plastic deformation for advanced properties, Nat. Mater. 3 (2004) 511–516.
[11] S. Bagheri, M. Guagliano, Review of shot peening processes to obtain nanocrystalline surfaces in metal alloys, Surf. Eng. 25 (2009) 3–14.
[12] S. Bagherifard, I. Fernandez-Pariente, R. Ghelichi, M. Guagliano, Severe shot peening to obtain nanostructured surfaces: process and properties of the treated surfaces, Handb. Mech. Nanostructuring (2015) 299–323.
[13] S. Bagherifard, I. Fernandez-Pariente, R. Ghelichi, M. Guagliano, Fatigue behavior of notched steel specimens with nanocrystallized surface obtained by severe shot peening, Mater. Des. 45 (2013) 497–503.
[14] S. Bagherifard, M. Guagliano, Fatigue behavior of a low-alloy steel with nanostructured surface obtained by severe shot peening, Eng. Fract. Mech. 81 (2012) 56–68.
[15] H. Hermawan, D. Ramdan, J.R.P. Djuansjah, Metals for Biomedical Applications, Biomedical Engineering – From Theory to Applications, 2011.
[16] S. Bagherifard, R. Ghelichi, M. Guagliano, A numerical model of severe shot peening (SSP) to predict the generation of a nanostructured surface layer of material, Surf. Coat. Technol. 204 (2010) 4081–4090.
[17] C.A. Schneider, W.S. Rasband, K.W. Eliceiri, NIH Image to Imagej: 25 years of image analysis, Nat. Methods 9 (2012) 671–675.
[18] H. Rietveld, A profile refinement method for nuclear and magnetic structures, J. Appl. Crystallogr. 2 (1969) 65–71.
[19] L. Lutterotti, S. Matthies, H.-R. Wenk, A. Schultz, J. Richardson Jr., Combined texture and structure analysis of deformed limestone from time-of-flight neutron diffraction spectra, J. Appl. Phys. 81 (1997) 594–600.
[20] N. Popa, The (hkl) dependence of diffraction-line broadening caused by strain and size for all laue groups in rietveld refinement, J. Appl. Crystallogr. 31 (1998) 176–180.
[21] ISO 4287: Geometrical Product Specifications (GPS) – Surface Texture: Profile Method Terms, Definitions and Surface Texture Parameters, first ed., 1997.
[22] F. Yan, G. Liu, N. Tao, K. Lu, Strength and ductility of 316L austenitic stainless steel strengthened by nano-scale twin bundles, Acta Mater. 60 (2012) 1059–1071.
[23] A. Hamada, L. Karjalainen, High-cycle fatigue behavior of ultrafine-grained austenitic stainless and TWIP steels, Mater. Sci. Eng. A 527 (2010) 5715–5722.

[24] B.D. Cullity, S.R. Stock, Elements of X-ray Diffraction, Pearson, 2001.
[25] S. Bagherifard, R. Ghelichi, M. Guagliano, Numerical and experimental analysis of surface roughness generated by shot peening, Appl. Surf. Sci. 258 (2012) 6831–6840.
[26] K.A. Kilian, B. Bugarija, B.T. Lahn, M. Mrksich, Geometric cues for directing the differentiation of mesenchymal stem cells, Proc. Natl. Acad. Sci. 107 (2010) 4872–4877.
[27] T.D. Brown, Techniques for mechanical stimulation of cells in vitro: a review, J. Biomech. 33 (2000) 3–14.
[28] T.J. Webster, J.U. Ejiofor, Increased osteoblast adhesion on nanophase metals: Ti, Ti6Al4V, and CoCrMo, Biomaterials 25 (2004) 4731–4739.
[29] S. Jindal, R. Bansal, B.P. Singh, R. Pandey, S. Narayanan, M.R. Wani, et al., Enhanced osteoblast proliferation and corrosion resistance of commercially pure titanium through surface nanostructuring by ultrasonic shot peening and stress relieving, J. Oral Implant. 40 (2014) 347–355.
[30] S.P. Xavier, P.S. Carvalho, M.M. Beloti, A.L. Rosa, Response of rat bone marrow cells to commercially pure titanium submitted to different surface treatments, J. Dent. 31 (2003) 173–180.
[31] I. Izquierdo-Barba, J.M. García-Martín, R. Álvarez, A. Palmero, J. Esteban, C. Pérez-Jorge, et al., Nanocolumnar coatings with selective behavior towards osteoblast and staphylococcus aureus proliferation, Acta Biomater. 15 (2015) 20–28.
[32] M. Bigerelle, K. Anselme, Statistical correlation between cell adhesion and proliferation on biocompatible metallic materials, J. Biomed. Mater. Res. Part A 72 (2005) 36–46.
[33] J. Lincks, B. Boyan, C. Blanchard, C. Lohmann, Y. Liu, D. Cochran, et al., Response of MG63 osteoblast-like cells to titanium and titanium alloy is dependent on surface roughness and composition, Biomaterials 19 (1998) 2219–2232.
[34] O. Zinger, G. Zhao, Z. Schwartz, J. Simpson, M. Wieland, D. Landolt, et al., Differential regulation of osteoblasts by substrate microstructural features, Biomaterials 26 (2005) 1837–1847.
[35] M. Ribeiro, F.J. Monteiro, M.P. Ferraz, Infection of orthopedic implants with emphasis on bacterial adhesion process and techniques used in studying bacterial-material interactions, Biomatter 2 (2012) 176–194.
[36] I.C. Sutcliffe, A phylum level perspective on bacterial cell envelope architecture, Trends Microbiol. 18 (2010) 464–470.
[37] S. Faghihi, A.P. Zhilyaev, J.A. Szpunar, F. Azari, H. Vali, M. Tabrizian, Nanostructuring of a titanium material by high-pressure torsion improves pre-osteoblast attachment, Adv. Mater. 19 (2007) 1069–1073.
[38] S. Faghihi, F. Azari, A.P. Zhilyaev, J.A. Szpunar, H. Vali, M. Tabrizian, Cellular and molecular interactions between MC3T3-E1 pre-osteoblasts and nanostructured titanium produced by high-pressure torsion, Biomaterials 28 (2007) 3887–3895.
[39] F. Nie, Y. Zheng, S. Wei, C. Hu, G. Yang, In vitro corrosion, cytotoxicity and hemocompatibility of bulk nanocrystalline pure iron, Biomed. Mater. 5 (2010) 065015.